Check for updates

Pseudo-*Para*-Substituted [2.2]Paracyclophanes for Hole Transport in Perovskite Solar Cells

Steffen A. Otterbach, David Elsing, Alexander D. Schulz, Henrik Tappert, Wolfgang Wenzel, Mariana Kozlowska, Holger Röhm,* and Stefan Bräse*

2,2′,7,7′-Tetrakis(*N,N*-di-*p*-methoxyphenylamine)—9,9′-spirobifluorene (spiro-OMeTAD) is the prevalent hole transport layer in perovskite solar cells (PSCs) with regular device architecture. Yet, its spirobifluorene core and multistep synthesis make it rather expensive. For the further technological success of PSCs, novel scalable and inexpensive alternative hole transport layers are needed. Herein, a study of the structure-property relations of pseudo-*para*-substituted [2.2]paracyclophanes is presented. Eight different hole transport materials are synthesized via double CH activation, eliminating metal-containing substituents for cross-coupling reactions. The ionization potentials (IPs) of the disubstituted paracyclophanes (DiPCPs) are examined by photoelectron spectroscopy in air, cyclic voltammetry and theoretical calculations. Through variation of donor groups and π-linkers, IPs that span a range from 5.14 to 5.86 eV are achieved, demonstrating high customizability. From the eight novel materials, five showed good solubility and are implemented into PSCs. The solar cells with a hole transport layer of undoped 4,16-di(4-(2-thienyl)-*N,N*-bis(4-methoxyphenyl)aniline)[2.2]paracyclophane (DiPCP-2) exhibit a power conversion efficiency of 12.7% ± 0.4%. The facile synthesis of DiPCP-2 enables an estimated cost reduction by two thirds compared to spiro-OMeTAD.

1. Introduction

The transition from fossil fuels to renewable energy sources has been one of the major research endeavors in the last decades. The global solar irradiation exceeds the world's energy demand 7500-fold and renders photovoltaics one of the central pillars of the energy transition.[1] A variety of different materials has been investigated as alternatives to the market dominating monocrystalline silicon.[2] Recently a new class of solar cells has emerged that rivals the power conversion efficiency (PCE) of silicon while demanding much less energy for production: Organic-inorganic lead halide PSCs have undergone rapid development since their discovery by Kojima et al. in 2009 and have now reached record PCEs of >25%.[3,4] The high PCEs of solar cells comprising perovskites as light-harvesting materials are based on low charge carrier recombination rates and efficient charge transport as evidenced by electron-hole diffusion lengths on the micrometer scale.[5–9] The perovskite layer is sandwiched in between the electron transport layer (ETL) facilitating electron extraction and the hole transport layer (HTL) facilitating hole extraction. In regular architecture PSCs, TiO_2 and SnO_2 are the most common ETLs. For this work, SnO_2 nanoparticles were chosen as the ETL because of their low processing temperature.[10–12] Their surface was modified with 4-(1′,5′-Dihydro-1′-methyl-2′*H*-[5,6]fullereno-C60-I_h-[1,9-c]-pyrrol-2′-yl)-benzoic acid (C60-SAM) in order to improve the stability of the perovskite at the interface (**Figure 1**).[13]

S. A. Otterbach, H. Tappert, S. Bräse
Institute of Organic Chemistry (IOC)
Karlsruhe Institute of Technology (KIT)
Fritz-Haber-Weg 6, 76131 Karlsruhe, Germany
E-mail: braese@kit.edu

D. Elsing, W. Wenzel, M. Kozlowska
Institute of Nanotechnology (INT)
Karlsruhe Institute of Technology (KIT)
Kaiserstraße 12, 76131 Karlsruhe, Germany

A. D. Schulz, H. Röhm
Light Technology Institute (LTI)
Karlsruhe Institute of Technology (KIT)
Engesserstrasse 13, 76131 Karlsruhe, Germany
E-mail: holger.roehm@kit.edu

A. D. Schulz, H. Röhm, S. Bräse
Material Research Center for Energy Systems (MZE)
Karlsruhe Institute of Technology (KIT)
Strasse am Forum 7, 76131 Karlsruhe, Germany

S. Bräse
Institute of Biological and Chemical Systems – Functional Molecular Systems (IBCS-FMS)
Karlsruhe Institute of Technology (KIT)
Hermann-von-Helmholtz-Platz 1, 76344 Eggenstein-Leopoldshafen, Germany

**ADVANCED
SCIENCE NEWS**

www.advancedsciencenews.com

**ADVANCED
FUNCTIONAL
MATERIALS**

www.afm-journal.de
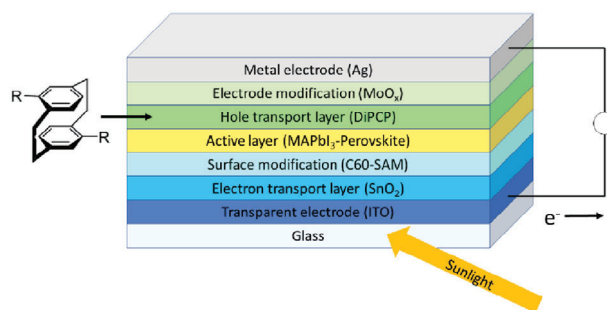
Figure 1. PSC architecture with novel disubstituted [2.2]paracyclophane (DiPCP) as the hole transport layer (HTL).

Just like ETLs, HTLs should have large optical bandgaps that prevent parasitic absorption of light, exhibit excellent conductivity and passivate defects on the perovskite surface.[14] Not least, properties such as stability against decomposition and solubility in solvents that are compatible with processing on the perovskite surface have to be considered for device manufacturing. The current benchmark for HTLs in regular architecture PSCs is 2,2′,7,7′-tetrakis(*N*,*N*-di-*p*-methoxyphenylamine)−9,9′-spirobifluorene (spiro-OMeTAD). Spiro-OMeTAD possesses a low intrinsic hole mobility and hence low conductivity,[15] but its conductivity can be enhanced via doping, which enables PCEs of >23%.[16] Doping further allows its use in relatively thick HTLs, which are often required in order to fully cover the surface of uneven perovskite layers. However, the synthesis of spiro-OMeTAD remains challenging for simple and low-cost application at an industrial scale, which calls for the exploration of alternatives.[17–20] Small changes in the structure of the molecules employed as HTLs, such as different substituents or substituent patterns, can strongly influence the ionization potential (IP) and other material properties.[21–23] Similar compounds such as spiro-linked molecules,[24] together with a variety of other cores such as acenes,[25–27] pyrenes,[28] or triphenylamines (TPAs) have been investigated,[29,30] but no clear successor to spiro-OMeTAD has been identified so far.

This prompted us to explore the emerging class of [2.2]paracyclophanes (PCPs) for hole transport in PSCs. PCPs consist of two aromatic benzene rings that are connected via ethylene bridges with a distance between the rings of only 3.09 Å (Figure S1, Supporting Information). The close vicinity of the two aromatic rings allows through-space conjugation,[31] and thus, the electron density can be spread over both rings and their substituents. In PSCs, [2.2]paracyclophane was first used as an HTL in 2015 by Park and coworkers with a bis(pseudo-*meta*)-*para* substitution of methoxy-substituted triphenylamines.[32] The PCP core promotes tight packing of molecules in thin-films, while the triphenylamine side groups enhance the solubility and charge transport properties. The role of the functional groups added to the PCP cores is their donor effect, which results in shallowing of the ionization potentials and the change in solubility. More specifically, the methoxy group donates electron density to the *π*-electron system through mesomeric effects, while the tert-butyl group shifts electron density to the donor due to its inductive effect. Both groups are known to increase solubility because they prevent aggregation through steric effects and promote interac-

tions with the solvents. In 2016, Park and coworkers compared the photovoltaic performances of a trisubstituted PCP-TPA and a tetrasubstituted PCP-TPA with a linear di(bis(4-methoxyphenyl) aniline-substituted benzene.[33] In 2021, Lin and coworkers investigated the influence of an alkene connecting the TPA donor group with PCP.[34] They reported that the overall PSC performance increased for the bis(pseudo-*meta*)-*para*-substituted PCP with a *π*-linker. In light of the high versatility of this material class, a vast amount of promising structures and facile synthesis routes remains yet to be explored.

In this work, we investigate the structure-property relation of pseudo-*para*-substituted PCP incorporating different donor groups and *π*-linkers. Donor groups leveraging inductive and mesomeric effects are synthesized and coupled with two *π*-linkers (thiophene or 3,4-ethylendioxythiophene (EDOT)). The [2.2]paracyclophane derivatives are synthesized via CH activation, which enables a more direct synthesis than the commonly used cross coupling methods, and thus saves resources and energy in the process.[35] The derivatives are investigated for their optical properties and IPs using absorption and emission spectroscopy, cyclic voltammetry (CV) and photoelectron spectroscopy in air (PESA). These efforts are supported by theoretical calculations, which guide data interpretation. Moreover, a transferrable method to quickly predict the properties of newly designed molecules using an automated workflow is developed. The results of those calculations help to promote a better understanding of the structure-property-relations and hence the design of PCP HTLs.
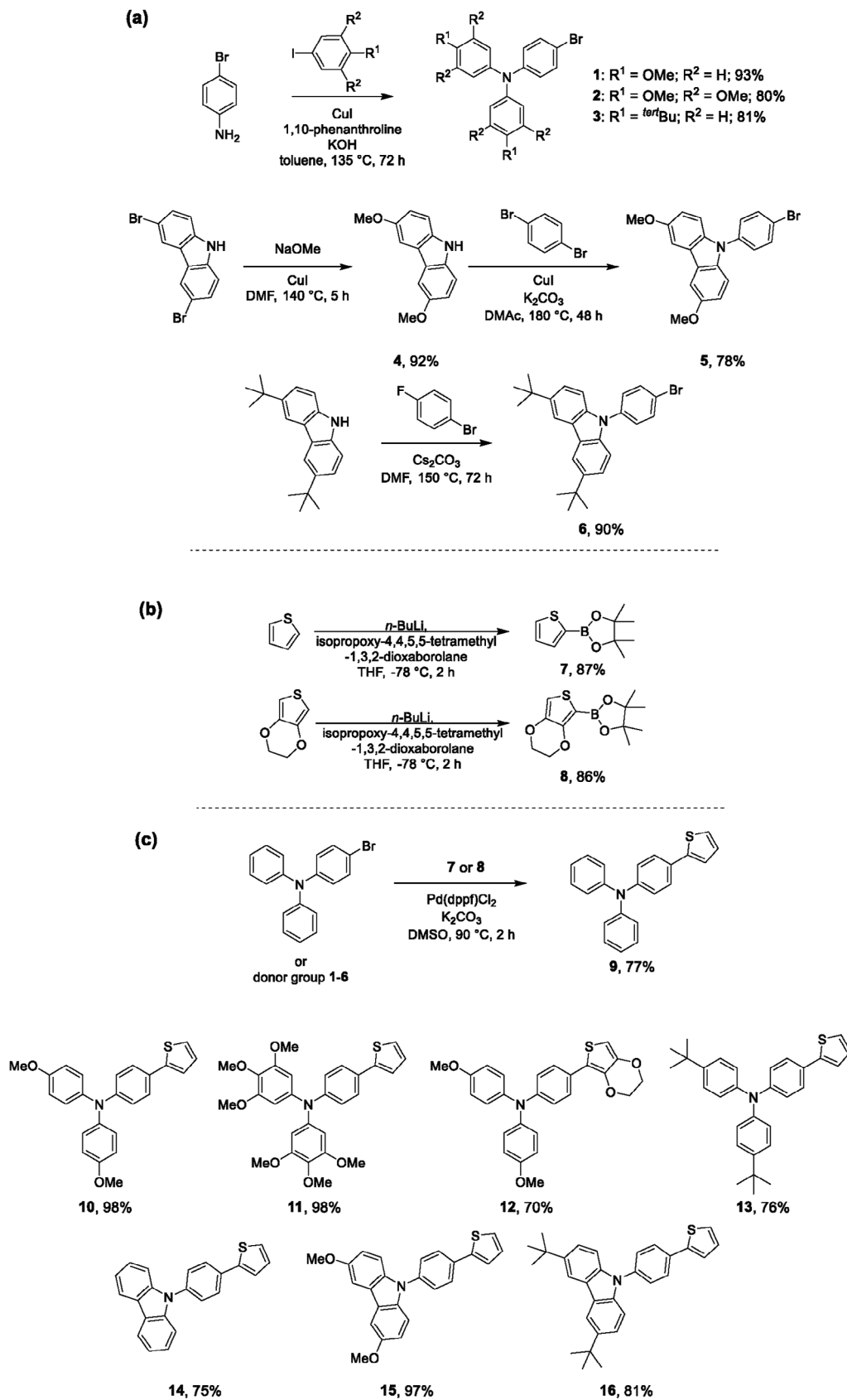
The charge carrier transport in undoped HTLs depends on good hole mobility. In order to quantify the hole mobility of the novel PCPs, we employ metal insulator semiconductor charge extraction by linearly increasing voltage (MIS-CELIV). With fundamental HTL properties understood, we finally implement DiPCP HTLs with sufficient solubility in chlorobenzene (CB) into PSCs and evaluate the solar cell performances.
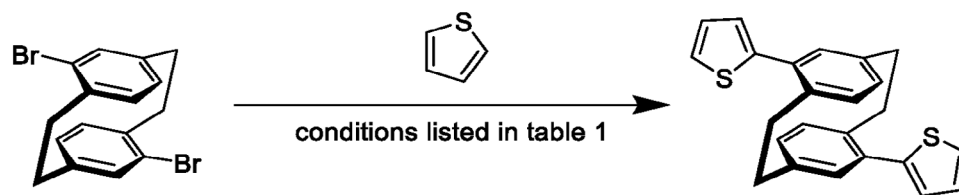
2. Results and Discussion

2.1. Synthesis

2.1.1. Synthesis of the Donor-π-Molecules

A variety of [2.2]paracyclophane derivatives featuring different donor groups was synthesized, and their structure-property relations were investigated. Both triphenylamines and carbazoles are common donors used in HTLs, since their IPs closely match with the typical IPs of light-harvesting perovskites. Furthermore, they are easy to synthesize and functionalize. Two functionalizations introduced in this work are methoxy and *tert*-butyl moieties, which feature mesomeric and inductive donor effects, respectively. This provides an additional handle to modify the IPs. For the triphenylamine-based donors, an Ullmann-type condensation was performed, using 4-bromoaniline and different substituted iodobenzenes, following a procedure published by Li and coworkers for 4-iodoanisole.[36] Three different substituted triphenylamines were synthesized, with methoxy substituents (+M- and -I effect) in *para*-position (1), in *meta*- and *para*-position (2) and *tert*-butyl substituents in *para*-position (3) (**Scheme 1**a). For comparison, two carbazole-containing donors with analogous

**ADVANCED
SCIENCE NEWS**

www.advancedsciencenews.com

**ADVANCED
FUNCTIONAL
MATERIALS**

www.afm-journal.de

Scheme 1. Synthesis of donor-π-molecules.

Scheme 2. Test system for optimization of CH activation.

substitution were also synthesized. Both carbazoles, methoxy-substituted (**5**) and *tert*-butyl-substituted (**6**) were synthesized according to published procedures (Scheme 1a).[37–39]

For the synthesis of the donor-π-molecules, the π-linkers thiophene and EDOT were first borylated in the 2-position with *n*-BuLi and the subsequent addition of 2-isopropoxy-4,4′,5,5′-tetramethyldioxoborolane to yield 2-pinacolborylthiophene (**7**) and 2-pinacolboryl-3,4-ethylendioxythiophene (**8**) with satisfying yields of 87% and 86% (Scheme 1b).[40] With the borylated π-bridges successfully synthesized, the Suzuki-Miyaura palladium-catalyzed cross-coupling reactions with the donor groups were carried out under typical reaction conditions, particularly dimethyl sulfoxide as the solvent, Pd(dppf)Cl₂ as catalyst and potassium carbonate as the base. In addition to the synthesized donor groups, the unsubstituted triphenylamine as well as the unsubstituted carbazole were used for the coupling. Overall, eight different donor-π-molecules were synthesized with yields between 98% and 70% (Scheme 1c), with one molecule containing EDOT as the π-linker (**12**).

2.1.2. Synthesis of the PCP-Containing HTMs

In a first step, different palladium-catalyzed CH activation conditions, known from the literature, were tested to optimize the yield of the desired products.[29,41–43] 4,16-dibromo PCP was used as starting material and coupled with thiophene, while varying the solvent, the temperature, the equivalents of thiophene, the catalyst, the base and the additives (**Scheme 2**). The results are summarized in **Table 1**.

The highest isolated yield of 4,16-dithienyl-[2.2]paracyclophane was achieved with a combination of different literature-known procedures for CH activations, combining Pd(OAc)₂, P(Ph)₃ and pivalic acid (PivOH) in *N,N*-dimethylformamide (DMF) at 100 °C with 20.0 equivalents of thiophene and a reaction time of 48 h. Due to the low boiling point of thiophene (87 °C), the equivalents of the donor-π-molecule were reduced to 2.20 for the coupling of the donor-π-molecules with 4,16-dibromo-PCP. The desired target materials were isolated after a reaction time of 18 h and after a first purification via column chromatography, the pure products were obtained by precipitation from a cyclohexane/dichloromethane mixture (**Scheme 3**). All eight donor-π-molecules were successfully used and introduced to the paracyclophane core, making it the first double CH activation with a [2.2]paracyclophane core. With the successful synthesis via CH activation, expensive and metal-containing Suzuki-Miyaura-, Kumada-, or Stille-reagents become obsolete, allowing easier and cheaper synthesis. The yields ranged between 24% and 62% and the purity was con-

firmed via ¹H NMR, ¹³C NMR, HSQC, IR spectroscopy and mass spectrometry. The experimental procedures and analytic data are provided in the supporting information (SI).

To prove the competitiveness of this synthesis, we estimated the cost of the molecule **DiPCP-2** as an example and compared it to spiro-OMeTAD. While the estimations, following the model of Osedach et al.,[44] are rough and costs naturally vary by region, they give a good relative scale. The calculated cost for 1 g of **DiPCP-2** is 91 $US (Tables S10–S13, supporting information) while the cost for spiro-OMeTAD is estimated at 274 $US.[45] This means that the production cost of **DiPCP-2**, even though its synthesis was optimized for yield and practicability, is only a third of the costs of spiro-OMeTAD.
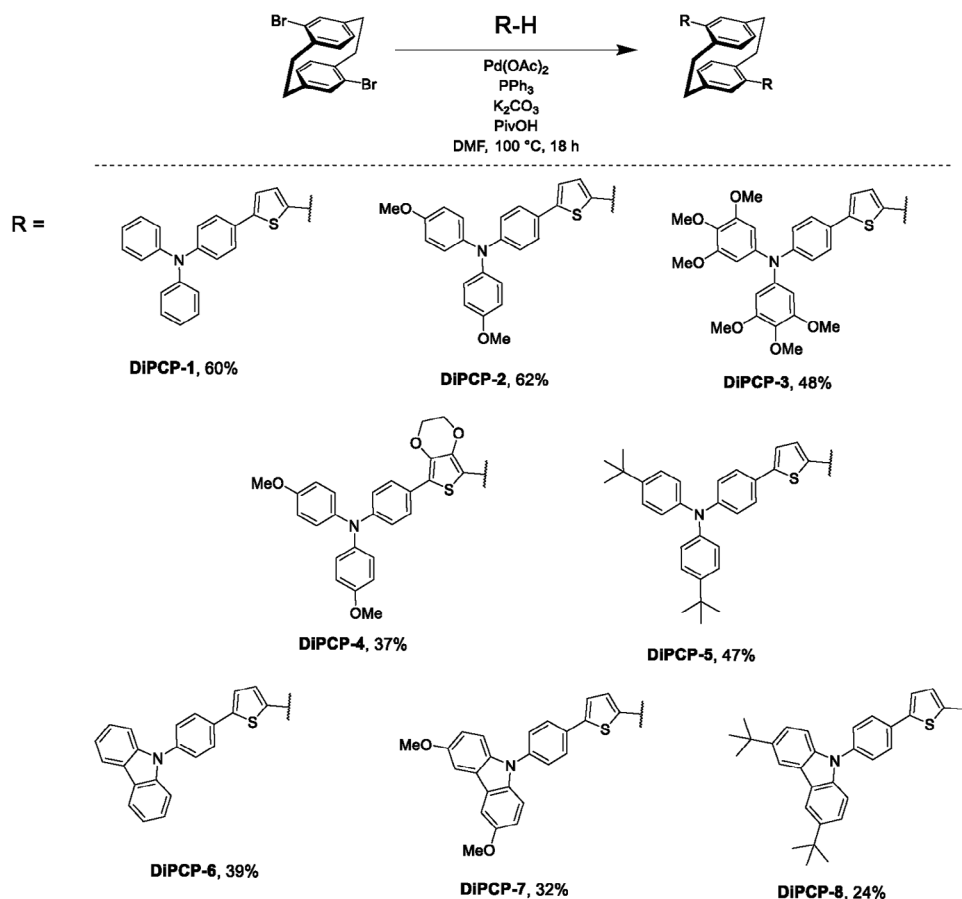
2.2. Theoretical Calculations

The theoretical calculations of the electronic properties of the disubstituted [2.2]paracyclophanes were performed for multiple conformers of each molecule by the developed, automated workflow using Snakemake.[46] This workflow is fully transferrable to other classes of molecules. As the DiPCP molecules are quite flexible, the conformational space was thoroughly explored using different levels of theory as shown in **Figure 2**.

Initially, conformers were generated by the ETKDG (experimental-torsion distance geometry with basic knowledge) method[47] as implemented in RDKit[48] and later optimized with the Merck molecular force field.[49] They were then used as inputs for the CREST (Conformer–Rotamer Ensemble Sam-

Table 1. Overview of different CH activation conditions for the coupling of *psp*-Br2-PCP with thiophene.

Entry	Thiophene [equiv.]	Catalyst	Ligand	Additive	Temperature [°C]	Solvent	Yield [%]
1	2.50	Pd(OAc)₂	P(*m*-Tol)₃	–	110	Toluene	0
2	5.00	Pd(OAc)₂	P(*m*-Tol)₃	–	110	Toluene	0
3	10.0	Pd(OAc)₂	P(*m*-Tol)₃	–	110	Toluene	0
4	20.0	Pd(OAc)₂	P(*m*-Tol)₃	–	110	Toluene	**42**
5	20.0	Pd(OAc)₂	P(Ph)₃	–	110	Toluene	0
6	20.0	Pd(OAc)₂	P(Cy)₃	PivOH	110	DMF	0
7	20.0	Pd(OAc)₂	P(Ph)₃	PivOH	100	DMF	**71**
8	4.00	Pd(OAc)₂	P(Ph)₃	PivOH	100	DMF	**12**
10	4.00	Pd(dppf)Cl₂	–	PivOH	100	DMF	0
11	4.00	Pd(dppf)Cl₂	–	–	100	DMF	0
12	4.00	Pd(PPh₃)₄	–	PivOH	100	DMF	0
13	4.00	Pd(PPh₃)₄	–	–	100	DMF	0

ADVANCED
SCIENCE NEWS

www.advancedsciencenews.com

ADVANCED
FUNCTIONAL
MATERIALS

www.afm-journal.de

Scheme 3. Synthesis of the DiPCP derivatives.

pling Tool) program[50] using the GFN-FF force field[51] for the sampling and energy calculation (Figure 2, blue box). To exclude duplicate conformers, and conformers with high structural similarity, a root-mean-square deviation (RMSD) threshold of 0.125 Å with the energy threshold (above which conformers are treated as distinct) of 0.05 kcal mol^{-1} was used to filter initially generated conformers.
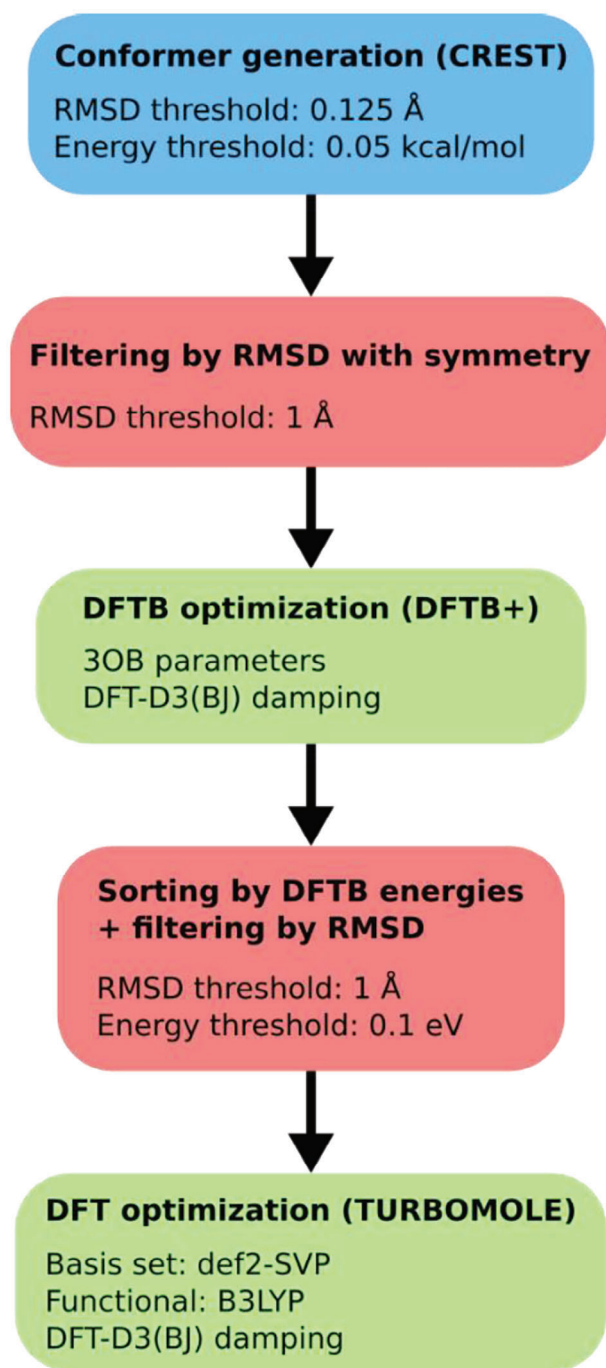
Since the RMSD algorithm used in the CREST code is not symmetry-corrected, the generated conformers (between 84 and 900 conformers for each molecule) were additionally filtered by symmetry-corrected RMSD with a threshold of 1 Å.[52] Here, the RMSD between two conformers was minimized over rotations, reflections and the atom permutations in the automorphism group of the molecular graph, ignoring the hydrogen atoms. This resulted in 15–69 distinct conformers (obtained after the second step, marked in red after CREST) that were used for the next steps of geometry optimization. Next, all remaining conformers were optimized by the Density Functional based Tight Binding (DFTB) using DFTB+ program,[53] the 3OB parameters[54,55] and the corresponding Grimme DFT-D3 dispersion correction[56] with BJ damping (Figure 2, third box in green).[57,58] Afterwards, they were filtered again for the selection of ten distinct conformers for each molecule. For the filtering algorithm, the DFTB energies were considered: The conformers were sorted by the energies beforehand, and conformers, which differed by >0.1 eV in their

DFTB energies, were treated as distinct regardless of RMSD. This scheme guarantees that the conformers used as input for the expensive DFT (Density Functional Theory) calculations really are distinct and the conformational space is efficiently sampled. Since the force field energies are generally rather inaccurate,[59] the energy sorting is done only with the DFTB energies.

All DFT calculations for the selected ten conformers of each of the molecules (i.e., final geometry optimization, calculation of orbitals and potentials) were performed using Turbomole, version 7.4.1.[60] The geometry optimizations were performed with the def2-SVP basis set[61] and the B3LYP functional,[62–65] using the Grimme DFT-D3 dispersion correction[56] with BJ damping.[57] For the electronic properties of the final conformers, the def2-TZVP[66] basis set was used, again with the B3LYP functional and DFT-D3(BJ) dispersion correction. Additionally, the multipole accelerated Resolution of Identity approximation for the Coulomb term[67–73] was applied in all cases.

Using the optimized structures, electronic properties were calculated. The IP was obtained as the difference between the total DFT energy for charge +1 and the total energy for the neutral molecule. Likewise, the electron affinity of all molecules was calculated as the difference between the energy of the neutral molecule and of the negatively charged molecule (charge −1). To investigate the polarization influence of the solvent on the electronic properties of molecules, calculations with the COSMO

**ADVANCED
SCIENCE NEWS**

www.advancedsciencenews.com

**ADVANCED
FUNCTIONAL
MATERIALS**

www.afm-journal.de

Conformer generation (CREST)

RMSD threshold: 0.125 Å
Energy threshold: 0.05 kcal/mol

↓

Filtering by RMSD with symmetry

RMSD threshold: 1 Å

↓

DFTB optimization (DFTB+)

3OB parameters
DFT-D3(BJ) damping

↓

**Sorting by DFTB energies
+ filtering by RMSD**

RMSD threshold: 1 Å
Energy threshold: 0.1 eV

↓

DFT optimization (TURBOMOLE)

Basis set: def2-SVP
Functional: B3LYP
DFT-D3(BJ) damping

Figure 2. Scheme of the conformer generation workflow.

(conductor-like screening) implicit solvent model[74,75] were performed with a relative permittivity of $\varepsilon = 37.315$[76] for DMF. Only the lowest conformer of each of the molecules was considered. Implicit solvation with $\varepsilon = 3$, which we assume to be characteristic for thin films, was also calculated. A complete overview of calculated electronic data is given in Table S1 and Figures S5–S7 (Supporting Information). The first singlet excitation energies (for the neutral molecules) were calculated with time-dependent DFT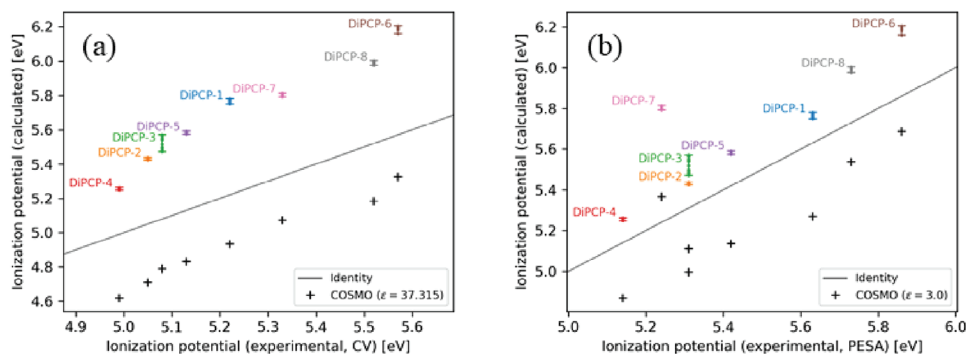[77–80] using B3LYP/def2-TZVP. In Tables S2–S9 (Supporting Information), the energies and oscillator strength (velocity form) of the lowest singlet-singlet excitations and their dominant contributions are shown for the lowest-energy conformer of each of the molecules. The electron density difference upon the first singlet excitation, showing electron donating and electron accepting fragments of the DiPCPs is visualized in Figures S7–S9 (Supporting Information).

Tuned DFT functionals may show better agreement with experiments, however this was not in the scope of the present paper. To check the usability of the results as a prediction tool for new PCP HTLs, they must be compared to the measured values of the synthesized molecules, which will be discussed in detail in the following chapter.

2.3. Optical and Electronic Characterization

In order to experimentally determine the IPs of all eight novel DiPCP compounds we used two different methods: PESA and CV. PESA was performed on spin-coated thin-films and hence in the same state of aggregation that prevails in a solar cell. In a nutshell, samples are irradiated with monochromatic UV photons of successively increasing energy. If the photon energy exceeds the energy required for electrons to escape the sample, they are ejected as photoelectrons and collected by an open-air counter.[81] An increase in the occupied density of states results in an increased photoelectron yield and by fitting the photoelectron yield against the photon energy, the IP can be obtained.[82] CV measures the required voltage for oxidation and reduction processes against a reference, often ferrocene, in a solvent. From those the IP and electron affinity of the non-aggregated compounds can be derived. Since CV is performed on a solute in an environment of polar solvent and electrolyte, it consistently measures lower IPs than PESA.[83,84] **Figure 3**a shows the correlation between the CV measurements conducted in DMF solution and the simulations both with and without an implicit solvent environment ($>\varepsilon$). Likewise, Figure 3b shows the correlation between PESA measurements conducted on a solid thin film and the simulations both with and without an implicit thin film environment ($<\varepsilon$). PESA measurements of all DiPCP compounds are summarized in Figures S10 and S11 (Supporting Information), while the graphs of oxidative and reductive CV measurements can be found in Figure S12 (Supporting Information). Generally, the IPs in vacuum as obtained from DFT calculations are higher than the IPs found by CV and PESA. The correlation between PESA and the calculations is more consistent with differences in the range of 0.1–0.3 eV with the exception of **DiPCP-7**, which shows higher deviation of 0.57 eV (Figure 3b). The inclusion of the polarizable environment into the DFT calculations (DMF used in CV; Figure 3a) or mimicking the permittivity of a thin film (used in PESA; Figure 3b) leads to lower IPs without a significant improvement of the correlation, now underestimating the IPs that were obtained from CV and PESA. Tuned DFT functionals may show better agreement with absolute values from experiments, but the relative IP trend is well represented by these simulations, demonstrating the usefulness of the developed workflow for further screening of a huge number of other possible molecules.

The experimentally obtained IPs of the eight DiPCP-based materials span a wide range, demonstrating good tunability by

**ADVANCED
SCIENCE NEWS**

www.advancedsciencenews.com

**ADVANCED
FUNCTIONAL
MATERIALS**

www.afm-journal.de

Figure 3. Comparison of experimental and calculated (DFT) IPs for both vacuum (colored) and implicit polarizable environments mimicking DMF for CV and the thin film for PESA (black crosses). a) IP from CV versus vacuum (DFT) versus $\varepsilon = 37.3$ (DFT). b) IP from PESA versus vacuum (DFT) versus $\varepsilon = 3.0$ (DFT).

changing the chemical composition of the donor-π-substituent. While the lowest IP was achieved for **DiPCP-4** with EDOT as the π-linker and triphenylamine as the donor group (CV: 4.99 eV, PESA: 5.14 eV), the corresponding compound **DiPCP-2** with a thiophene π-linker lies slightly higher (CV: 5.05 eV, PESA: 5.31 eV). An increase in the number of methoxy substituents only leads to a negligibly higher IP (DiPCP-3), but the use of *tert*-butyl instead of methoxy substitution increases the IP by $\approx$50–100 meV (**DiPCP-5**). The highest IPs are obtained without any substituents on the triphenylamine (**DiPCP-1**). The materials with carbazole as a donor group tend to have higher IPs compared to triphenylamine. Again, the lowest IP is obtained for the methoxy-substituted compound (**DiPCP-7**) due to the mesomeric donor effect of the methoxy moiety. The unsubstituted and the *tert*-butyl-substituted materials **DiPCP-6** and **DiPCP-8** have significantly deeper IPs >5.5 eV, and thus may impede hole extraction in methylammonium lead iodide (MAPbI$_3$) solar cells. Yet they are likely to fit other light-harvesting materials with deeper valence band energies. The obtained IPs from calculations, PESA and CV are summarized in **Table 2**.

In order to avoid parasitic light absorption in the HTL, the optical energy gap (E_g^{opt}) has to be reasonably large. Due to the placement of the HTL in regular architecture PSCs and the high ab-

sorption coefficient of the perovskite in the blue, $E_g^{opt} > 2$ eV is sufficient. We used UV–vis absorbance and photoluminescence (PL) measurements in solution to determine whether the DiPCPs fulfill this criterion. The spectra are plotted in **Figure 4**a,b. The main absorption band between 370 and 400 nm can be attributed to a $\pi \rightarrow \pi^*$ transition from the highest occupied molecular orbital (HOMO) to the lowest unoccupied molecular orbital (LUMO), depicted in Figures S8 and S9 (Supporting Information). According to our calculations, the HOMO of these molecules is delocalized mostly across the donor moiety and π-bridge, while the LUMO is delocalized across the π-bridge and the PCP core (Figure S5, Supporting Information). The transition orbitals and their contributions, describing the ten lowest excitations of the DiPCPs, are listed in Tables S2–S9 (Supporting Information). The carbazole-substituted HTLs tend to have wider energy gaps, and therefore blue-shifted absorption compared to the triphenylamine-substituted PCPs. We also observe a clear trend of the absorption maxima λ_{max} for substitution of the donor groups with *tert*-butyl and methoxy moieties: The two molecules with unsubstituted donors, **DiPCP-1** and **DiPCP-6**, have λ_{max} at the lowest wavelengths of 373 and 345 nm, respectively, while λ_{max} of the *tert*-butyl-substituted **DiPCP-2** and **DiPCP-8** are slightly red-shifted (by 8 and 6 nm) and the methoxy-substituted **DiPCP-2**, **DiPCP-3**, **DiPCP-4** and **DiPCP-7** show a

Table 2. Optical and electronic properties of all synthesized disubstituted [2.2]paracyclophanes: voltage of oxidation process in CV against ferrocene (E_{ox}^{CV}), ionization potential derived from CV data (E_{IP}^{CV}), ionization potential derived from PESA data (E_{IP}^{PESA}), ionization potential derived from DFT calculations in vacuum (E_{IP}^{calc}), wavelength of the absorbance maximum (λ_{max}), wavelength of the PL emission maximum (λ_{em}) and optical energy gap derived from the intersection of normalized absorbance and PL data (E_g^{opt}).

Compound	E_{ox}^{CV} [V vs Fc]	E_{IP}^{CV*} [eV]	E_{IP}^{PESA} [eV]	E_{IP}^{calc} [eV]	λ_{max} [nm]	λ_{em} [nm]	E_g^{opt} [eV]
DiPCP-1	0.41	5.22	5.63	5.77	373	452	2.96
DiPCP-2	0.25	5.05	5.31	5.43	384	482	2.88
DiPCP-3	0.28	5.08	5.31	5.57	383	467	2.90
DiPCP-4	0.19	4.99	5.14	5.26	386	455	2.94
DiPCP-5	0.33	5.13	5.42	5.59	381	450	2.97
DiPCP-6	0.77	5.57	5.86	6.21	345	455	3.01
DiPCP-7	0.53	5.33	5.24	5.81	372	455	3.03
DiPCP-8	0.72	5.52	5.73	6.00	351	455	3.04

*Potential ferrocene (Fc) ($E°(Fc^+/Fc) = 0.400$ V vs NHE).[85]
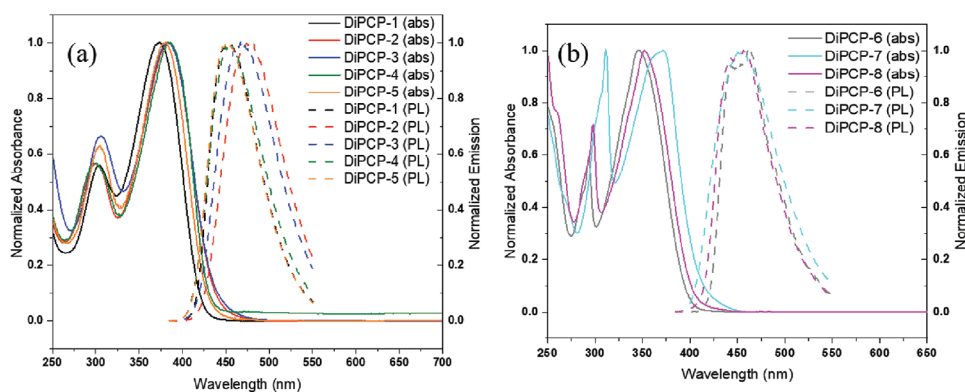
Figure 4. a) Normalized absorbance and PL spectra of triphenylamine-containing PCPs (in THF). b) Normalized Absorbance and PL spectra of carbazole-containing PCPs (in THF).

stronger red-shift of 13 nm between **DiPCP-1** and **DiPCP-4** and ≈30 nm between **DiPCP-6** and **DiPCP-7** (Table 2). This trend is in accordance with the HOMO/LUMO energies derived from the computational protocol described before. The measured PL spectra display emission between 450 and 480 nm. The intersection of the normalized absorbance and PL spectra is used to determine E_g^{opt}, as described by Chang et al.[29] Since all DiPCP HTLs only show significant absorbance below a wavelength of 430 nm (2.9 eV), parasitic absorption introduced into solar cells would be negligible. On top of preventing parasitic absorption, the large energy gaps also help to block electrons from the light-harvesting layer, thus making the HTLs more charge carrier selective.

2.4. Hole Mobility and Implementation of DiPCP in Solar Cells

Before applying the synthesized DiPCPs in thin-film devices, the solubility of all compounds in CB, which is compatible with deposition on top of perovskite layers, was determined. A solubility of at least 10 g L^{-1} was set as a gate criterion in order to enable fabrication of thin films with sufficient thickness for solar cells. Three materials did not exhibit sufficient solubility, that is, the unsubstituted **DiPCP-1** and **DiPCP-6** and the EDOT-containing **DiPCP-4**, which showed otherwise promising electronic properties (Table S5, Supporting Information). Assuming that the low solubility of **DiPCP-4** in CB is related to the polar nature of EDOT, we tested ethyl acetate as an alternative solvent. While a lot of polar solvents are incompatible to processing directly on the perovskite surface, water-free ethyl acetate can be used. Unfortunately, the solubility of **DiPCP-4** in ethyl acetate was <5 g L^{-1} hence not passing the required criterion either.

MIS-CELIV devices for measurements of the charge carrier mobility do not have the same solvent restriction. In order to achieve thick layers for more accurate mobility measurements, we dissolved **DiPCP-1** (saturated and filtered) and **DiPCP-7** (15 g L^{-1}) in chloroform, whereas for **DiPCP-2**, **DiPCP-3** and **DiPCP-5** solubility in CB was sufficiently high at >30 g L^{-1}. **DiPCP-4** was omitted due to its low solubility and **DiPCP-6** and **DiPCP-8** were omitted because of their high IPs, which would likely hinder formation of an ohmic contact with the top electrode. MIS-CELIV is selective for the charge carrier type not only

because of the work function of the injecting contact, but also because the polarity of the injection voltage that charges the semiconductor at the interface with the insulator layer. Furthermore, it requires only one ohmic contact, which can be the same contact as used in solar cells, rendering MIS-CELIV more reliable than the popular space-charge-limited current (SCLC) method.[86] Surprisingly, we could not inject charge carriers into **DiPCP-3**, even though its IP is similar to other tested compounds, where charge injection and extraction were successful. **Figure 5** shows the current transients obtained from MIS-CELIV measurements of the remaining DiPCPs with spiro-OMeTAD as a reference and the architecture as an inset.
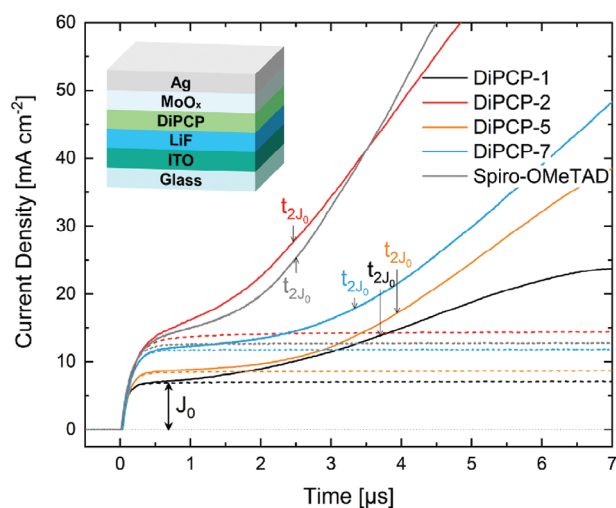

Figure 5. MIS-CELIV measurements of DiPCP compounds and reference spiro-OMeTAD. Measurements without any prior charge carrier injection (dashed lines) reveal large differences between the displacement currents J_0, which are related to differing layer thicknesses and relative permittivities. Upon application of an injection voltage before the measurement, a charge carrier reservoir is created at the semiconductor insulator interface (DiPCP/LiF), out of which charge carriers are extracted during the linear voltage ramp (starting at $t = 0$) as a space charge limited current (solid lines). The rise of the transient current is related to the charge carrier mobility, which is highest for **DiPCP-1**, followed by spiro-OMeTAD and **DiPCP-2**.

In short, holes are injected into the DiPCP layer through a molybdenum oxide/silver electrode, where they accumulate at the interface to an insulating lithium fluoride layer ($d_i = 20$ nm). Subsequently, a (reverse) linear voltage ramp ($A = 400$ mV μs^{-1}) is applied during which the charge carrier reservoir emits holes, which travel back through the DiPCP layer and are collected at the electrode from which they were injected before. The resulting current overlays the displacement current of the geometric capacitance J_0. From J_0 we calculated the relative permittivity of the semiconductor ε_s (Equation S1) and from t_{2J0} the charge carrier mobility μ (Equation S2).[87,88] A summary of the parameters is listed in **Table 3**. ε_s of the HTLs lies in a range from 3.8 to 4.1, except for DiPCP-3 and **DiPCP-5**, which feature lower ε_s of 3.3 ± 0.2 and 3.0 ± 0.2, respectively. Hence, the threefold methoxy substitution and the *tert*-butyl substitution make DiPCP-3 and **DiPCP-5** less polar than the unsubstituted **DiPCP-1** ($\varepsilon_s = 3.8 \pm 0.1$) and the methoxy-substituted **DiPCP-2** (3.9 ± 0.2). Exchanging the donor group triphenylamine (**DiPCP-2**) with carbazole (**DiPCP-7**) had a negligible impact on ε_s, which can be explained by the similarity of the structures. The largest charge carrier mobility was obtained for **DiPCP-1** at $(4.4 \pm 0.2) \times 10^{-5}$ cm^2 V^{-1} s^{-1}, outperforming the reference spiro-OMeTAD with a hole mobility of $(2.7 \pm 0.3) \times 10^{-5}$ cm^2 V^{-1} s^{-1}. Out of the more soluble DiPCPs, the methoxy-substituted **DiPCP-2** reaches the largest hole mobility at $(2.2 \pm 0.2) \times 10^{-5}$ cm^2 V^{-1} s^{-1}, while the *tert*-butyl substituted **DiPCP-5** and the carbazole containing **DiPCP-7** follow closely at $(1.7 \pm 0.2) \times 10^{-5}$ cm^2 V^{-1} s^{-1} and $(1.5 \pm 0.2) \times 10^{-5}$ cm^2 V^{-1} s^{-1}, respectively.

The hole mobilities that were obtained for these novel DiPCP molecules are comparable to that of spiro-OMeTAD, rendering them promising candidates as HTLs for perovskite solar cells. Hence, we integrated all DiPCPs with a solubility of at least 10 g L^{-1} in CB into MAPbI$_3$ solar cells. C60-SAM modified SnO$_2$ was employed as the ETL and MAPbI$_3$ was chosen as the light-harvesting perovskite layer. The same electrode as in MIS-CELIV measurements was added on top of the HTL since it forms an ohmic contact with **DiPCP-2**, **DiPCP-5**, **DiPCP-7** and Spiro-OMeTAD. For completeness, we also included **DiPCP-3**, which did not form an ohmic contact with the MoO$_x$/Ag top electrode in MIS-CELIV experiments and **DiPCP-8** with its exceptionally high IP. **Figure 6** shows representative J–V curves (de-
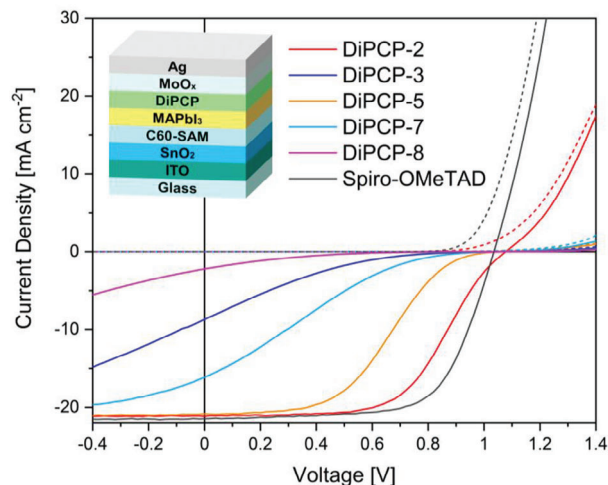
Figure 6. Representative J–V curves (descending scanning direction) of PSCs comprising DiPCP HTLs and reference spiro-OMeTAD under illumination (solid lines) and in the dark (dashed lines). S-shapes likely occur due to space charge accumulation.

scending direction), with the layer architecture depicted as an inset.

The solar cells with DiPCP HTLs exhibit differing degrees of s-shapes. Commonly, s-shapes are the result of space charge accumulation, which may stem from either a mismatch of the energy levels at the interface between the light-harvesting layer and the HTL, or from insufficient conductivity of the HTL. In either case, the space charges reduce the free energy gradient across the light-harvesting layer and hence hinder efficient charge extraction.[89] Furthermore, for **DiPCP-3**, we know from MIS-CELIV measurements that the contact to the top electrode is non-ohmic and the same is expected for **DiPCP-8** due to its high IP. Accordingly, they perform worst among the tested HTLs with PCEs of $1.0\% \pm 0.2\%$ and $0.2\% \pm 0.1\%$, respectively. The remaining DiPCPs and spiro-OMeTAD ($14.8\% \pm 0.5\%$) rank in order of their hole mobilities and IPs, with **DiPCP-2** ($12.7\% \pm 0.4\%$) performing best out of the DiPCPs, followed by **DiPCP-5** ($8.9\% \pm 0.6\%$) and **DiPCP-7** ($3.0\% \pm 0.3\%$). Notably, some of the DiPCP HTLs achieve larger open circuit voltages than spiro-OMeTAD, which indicates reduced surface recombination at the perovskite/HTL interface. In maximum power point tracking over ten minutes, the power output of the **DiPCP-2** and **DiPCP-5** hero devices remained stable, while the hero device with spiro-OMeTAD improved slightly (Figure S13, Supporting Information). Statistics of the solar cell parameters are summarized in **Table 4**, Figures S14 and S15 (Supporting Information). To understand whether the s-shapes can be explained by the differences in hole mobility, we performed supplementary device simulations (Figure S16, Supporting Information). The simulations show that hole mobilities on the order of 10^{-5} cm^2 V^{-1} s^{-1} can induce slight s-shapes. Yet, the strength of the experimentally observed s-shapes in the fourth quadrant (Figure 6) suggests that there are also energy alignment related extraction barriers. Furthermore, low current densities in the first quadrant are evident of injection barriers for **DiPCP-3**, **DiPCP-5**, **DiPCP-7**, and **DiPCP-8**. Improvement of charge carrier extraction is expected from future doping of the DiPCPs. The

Table 3. Summary of MIS-CELIV device parameters: semiconductor layer thickness d_s, displacement current J_0, time until twice the displacement current is reached t_{2J0}, semiconductor relative permittivity ε_s and hole mobility μ.

Compound	d_s [nm]	J_0 [mA cm^{-2}]	t_{2J0} [μs]	ε_s	μ [10^{-5} cm^2 V^{-1} s^{-1}]
DiPCP-1	183 ± 4	7.0	3.7	3.8 ± 0.1	4.4 ± 0.2
DiPCP-2	93 ± 5	13.9	2.5	3.9 ± 0.2	2.2 ± 0.2
DiPCP-3	74 ± 5	14.3	–	3.3 ± 0.2	–
DiPCP-5	120 ± 6	8.5	3.9	3.0 ± 0.2	1.7 ± 0.2
DiPCP-7	114 ± 6	11.7	3.3	4.1 ± 0.2	1.5 ± 0.2
Spiro-OMeTAD	104 ± 5	12.7	2.5	4.0 ± 0.2	2.7 ± 0.3

ADVANCED
SCIENCE NEWS
www.advancedsciencenews.com

ADVANCED
FUNCTIONAL
MATERIALS
www.afm-journal.de

Table 4. Solar cell parameters: Power conversion efficiency (PCE), fill factor, open circuit voltage (V_{OC}), and short circuit current density (J_{SC}) from descending (forward to reverse direction) and ascending (reverse to forward direction) J–V measurements. d_{HTL} is the layer thickness of the HTL. Solar cells with significant defects such as shorts were removed from the statistics (yield).

Compound	Scan direction	PCE[%]	Fill factor [%]	V_{OC}[mV]	J_{SC}[mA cm^{-2}]	d_{HTL}[nm]	Yield
DiPCP-2	Descending	12.7 ± 0.4	56 ± 2	1080 ± 10	21.0 ± 0.4	30 ± 4	11/16
	Ascending	11.7 ± 0.3	52 ± 1	1070 ± 10	20.9 ± 0.3		
DiPCP-3	Descending	1.0 ± 0.2	13 ± 1	1060 ± 20	7.8 ± 1.3	37 ± 1	7/16
	Ascending	0.7 ± 0.1	11 ± 1	1040 ± 10	6.4 ± 1.0		
DiPCP-5	Descending	8.9 ± 0.6	39 ± 2	1080 ± 10	21.1 ± 0.4	37 ± 2	15/16
	Ascending	8.6 ± 0.5	38 ± 2	1080 ± 10	21.0 ± 0.4		
DiPCP-7	Descending	3.0 ± 0.3	18 ± 1	1050 ± 30	15.9 ± 1.0	27 ± 2	14/16
	Ascending	2.5 ± 0.2	17 ± 1	1030 ± 30	14.3 ± 0.9		
DiPCP-8	Descending	0.2 ± 0.1	11 ± 1	1010 ± 20	2.1 ± 0.9	33 ± 1	11/16
	Ascending	0.2 ± 0.1	11 ± 1	910 ± 20	1.9 ± 0.8		
Spiro-OMeTAD	Descending	14.8 ± 0.5	68 ± 1	1030 ± 10	21.2 ± 0.5	N/A	13/16
	Ascending	13.2 ± 0.5	63 ± 1	1000 ± 20	21.0 ± 0.5		

DiPCP HTLs with particularly high IPs may be better suited for light-harvesting layers with higher IPs than MAPbI$_3$.

3. Conclusion

We demonstrated the synthesis, characterization and principal application of a variety of pseudo-*para*-substituted [2.2]paracyclophanes as HTLs in PSCs. Their structures were calculated using different levels of theory and conformer filtering schemes in an automated workflow protocol. The calculated IP trend showed good agreement with experiments: the donor effects of methoxy and *tert*-butyl substituents lead to significantly lower IPs (up to 600 meV difference) compared to the unsubstituted analogues. The wide range of IPs that was obtained shows great adaptability to match the energies of light-harvesting layers. DiPCP HTLs in this work were synthesized via double CH activation of thiophene, which is a fast and efficient process, lowering the total costs of **DiPCP-2** compared to spiro-OMeTAD by two thirds. Out of the compounds that were investigated, **DiPCP-2** is most promising because of excellent solubility and competitive hole mobility. In PSCs, a PCE of 12.7% ± 0.4% was achieved, which was only slightly below the PCE of devices with more expensive spiro-OMeTAD (14.8% ± 0.5%). Moreover, besides structural modification, doping of the HTLs may allow further enhancement of the device performance as is common in state-of-the-art PSCs. In the future, the computational protocol and automated workflow that were developed may be used for high-throughput screening of numerous HTL candidates.

4. Experimental Section

The synthetic and experimental procedures as well as theoretical calculations of all compounds are included in the supporting information.

Supporting Information

Supporting Information is available from the Wiley Online Library or from the author.

Conflict of Interest

The authors declare no conflict of interest.

Data Availability Statement

The data that support the findings of this study are available from the corresponding author upon reasonable request.

[1] W. E. Council, World Energy Resources: 2013 Survey, https://www.worldenergy.org/publications/entry/world-energy-resources-2013-survey, (accessed last: 31.03.2023).

[2] S. Almosni, A. Delamarre, Z. Jehl, D. Suchet, L. Cojocaru, M. Giteau, B. Behaghel, A. Julian, C. Ibrahim, L. Tatry, H. Wang, T. Kubo, S. Uchida, H. Segawa, N. Miyashita, R. Tamaki, Y. Shoji, K. Yoshida, N. Ahsan, K. Watanabe, T. Inoue, M. Sugiyama, Y. Nakano, T. Hamamura, T. Toupance, C. Olivier, S. Chambon, L. Vignau, C. Geffroy, E. Cloutet, et al., *Sci. Technol. Adv. Mater.* **2018**, *19*, 336.

[3] A. Kojima, K. Teshima, Y. Shirai, T. Miyasaka, *J. Am. Chem. Soc.* **2009**, *131*, 6050.

[4] M. A. Green, E. D. Dunlop, G. Siefer, M. Yoshita, N. Kopidakis, K. Bothe, X. Hao, *Prog. Photovoltaics* **2022**, *31*, 3.

[5] S. D. Stranks, G. E. Eperon, G. Grancini, C. Menelaou, M. J. P. Alcocer, T. Leijtens, L. M. Herz, A. Petrozza, H. J. Snaith, *Science* **2013**, *342*, 341.

[6] Q. Dong, Y. Fang, Y. Shao, P. Mulligan, J. Qiu, L. Cao, J. Huang, *Science* **2015**, *347*, 967.

[7] G. Xing, N. Mathews, S. Sun, S. S. Lim, Y. M. Lam, M. Grätzel, S. Mhaisalkar, T. C. Sum, *Science* **2013**, *342*, 344.

[8] M. Kim, G.-H. Kim, K. S. Oh, Y. Jo, H. Yoon, K.-H. Kim, H. Lee, J. Y. Kim, D. S. Kim, *ACS Nano* **2017**, *11*, 6057.

[9] Z. Song, C. L. McElvany, A. B. Phillips, I. Celik, P. W. Krantz, S. C. Watthage, G. K. Liyanage, D. Apul, M. J. Heben, *Energy Environ. Sci.* **2017**, *10*, 1297.

[10] L. Xiong, Y. Guo, J. Wen, H. Liu, G. Yang, P. Qin, G. Fang, *Adv. Funct. Mater.* **2018**, *28*, 1802757.

[11] Q. Jiang, X. Zhang, J. You, *Small* **2018**, *14*, 1801154.

[12] A. S. Subbiah, N. Mathews, S. Mhaisalkar, S. K. Sarkar, *ACS Energy Lett.* **2018**, *3*, 1482.

[13] I. M. Hermes, Y. Hou, V. W. Bergmann, C. J. Brabec, S. A. L. Weber, *J. Phys. Chem. Lett.* **2018**, *9*, 6249.

[14] W. Wang, J. Zhou, W. Tang, *J. Mater. Chem. A* **2022**, *10*, 1150.

[15] M. Maciejczyk, A. Ivaturi, N. Robertson, *J. Mater. Chem. A* **2016**, *4*, 4855.

[16] Q. Jiang, Y. Zhao, X. Zhang, X. Yang, Y. Chen, Z. Chu, Q. Ye, X. Li, Z. Yin, J. You, *Nat. Photonics* **2019**, *13*, 460.

[17] H. J. Snaith, M. Grätzel, *Appl. Phys. Lett.* **2006**, *89*, 262114.

[18] A. Abate, T. Leijtens, S. Pathak, J. Teuscher, R. Avolio, M. E. Errico, J. Kirkpatrik, J. M. Ball, P. Docampo, I. Mcpherson, H. J. Snaith, *Phys. Chem. Chem. Phys.* **2013**, *15*, 2572.

[19] C. Poriel, Y. Ferrand, S. Juillard, P. Le Maux, G. Simonneaux, *Tetrahedron* **2004**, *60*, 145.

[20] J. Salbeck, N. Yu, J. Bauer, F. Weissörtel, H. Bestgen, *Synth. Met.* **1997**, *91*, 209.

[21] Z. Hu, W. Fu, L. Yan, J. Miao, H. Yu, Y. He, O. Goto, H. Meng, H. Chen, W. Huang, *Chem. Sci.* **2016**, *7*, 5007.

[22] N. J. Jeon, H. G. Lee, Y. C. Kim, J. Seo, J. H. Noh, J. Lee, S. I. Seok, *J. Am. Chem. Soc.* **2014**, *136*, 7837.

[23] A. T. Murray, J. M. Frost, C. H. Hendon, C. D. Molloy, D. R. Carbery, A. Walsh, *Chem. Commun.* **2015**, *51*, 8935.

[24] I. M. Abdellah, T. H. Chowdhury, J.-J. Lee, A. Islam, M. K. Nazeeruddin, M. Grätzel, A. El-Shafei, *Sustainable Energy Fuels* **2021**, *5*, 199.

[25] M. Saliba, S. Orlandi, T. Matsui, S. Aghazada, M. Cavazzini, J.-P. Correa-Baena, P. Gao, R. Scopelliti, E. Mosconi, K.-H. Dahmen, F. De Angelis, A. Abate, A. Hagfeldt, G. Pozzi, M. Graetzel, M. K. Nazeeruddin, *Nat. Energy* **2016**, *1*, 15017.

[26] S. Kazim, F. J. Ramos, P. Gao, M. K. Nazeeruddin, M. Grätzel, S. Ahmad, *Energy Environ. Sci.* **2015**, *8*, 1816.

[27] H. D. Pham, H. Hu, F.-L. Wong, C.-S. Lee, W.-C. Chen, K. Feron, S. Manzhos, H. Wang, N. Motta, Y. M. Lam, P. Sonar, *J. Mater. Chem. C* **2018**, *6*, 9017.

[28] Q.-Q. Ge, J.-Y. Shao, J. Ding, L.-Y. Deng, W.-K. Zhou, Y.-X. Chen, J.-Y. Ma, L.-J. Wan, J. Yao, J.-S. Hu, Y.-W. Zhong, *Angew. Chem., Int. Ed.* **2018**, *57*, 10959.

[29] Y.-C. Chang, K.-M. Lee, C.-H. Lai, C.-Y. Liu, *Chem Asian J* **2018**, *13*, 1510.

[30] H. Choi, S. Park, S. Paek, P. Ekanayake, M. K. Nazeeruddin, J. Ko, *J. Mater. Chem. A* **2014**, *2*, 19136.

[31] Z. Hassan, E. Spuling, D. M. Knoll, J. Lahann, S. Bräse, *Chem. Soc. Rev.* **2018**, *47*, 6947.

[32] S. Park, J. H. Heo, C. H. Cheon, H. Kim, S. H. Im, H. J. Son, *J. Mater. Chem. A* **2015**, *3*, 24215.

[33] S. Park, J. H. Heo, J. H. Yun, T. S. Jung, K. Kwak, M. J. Ko, C. H. Cheon, J. Y. Kim, S. H. Im, H. J. Son, *Chem. Sci.* **2016**, *7*, 5517.

[34] Y.-S. Lin, H. Li, W.-S. Yu, S.-T. Wang, Y.-M. Chang, T.-H. Liu, S.-S. Li, M. Watanabe, H.-H. Chiu, D.-Y. Wang, Y. J. Chang, *J. Power Sources* **2021**, *491*, 229543.

[35] F. Roudesly, J. Oble, G. Poli, *J. Mol. Catal. A: Chem.* **2017**, *426*, 275.

[36] T.-Y. Li, C. Su, S. B. Akula, W.-G. Sun, H.-M. Chien, W.-R. Li, *Org. Lett.* **2016**, *18*, 3386.

[37] M. Holzapfel, C. Lambert, *J. Phys. Chem. C* **2008**, *112*, 1227.

[38] M. Mao, M.-G. Ren, Q.-H. Song, *Chemistry* **2012**, *18*, 15512.

[39] L. Wang, E. Ji, N. Liu, B. Dai, *Synthesis* **2016**, *48*, 737.

[40] Y. Dienes, S. Durben, T. Kárpáti, T. Neumann, U. Englert, L. Nyulászi, T. Baumgartner, *Chemistry* **2007**, *13*, 7487.

[41] C.-Y. Liu, H. Zhao, H.-H. Yu, *Org. Lett.* **2011**, *13*, 4068.

[42] C. Kieffer, V. Babin, M. Jouanne, I. Slimani, Y. Berhault, R. Legay, J. Sopková-De Oliveira Santos, S. Rault, A. S. Voisin-Chiret, *Tetrahedron* **2017**, *73*, 5509.

[43] M. Lafrance, K. Fagnou, *J. Am. Chem. Soc.* **2006**, *128*, 16496.

[44] T. P. Osedach, T. L. Andrew, V. Bulović, *Energy Environ. Sci.* **2013**, *6*.

[45] B. Pashaei, S. Bellani, H. Shahroosvand, F. Bonaccorso, *Chem. Sci.* **2020**, *11*, 2429.

[46] F. Molder, K. P. Jablonski, B. Letcher, M. B. Hall, C. H. Tomkins-Tinch, V. Sochat, J. Forster, S. Lee, S. O. Twardziok, A. Kanitz, A. Wilm, M. Holtgrewe, S. Rahmann, S. Nahnsen, J. Koster, *F1000Res* **2021**, *10*, 33.

[47] S. Riniker, G. A. Landrum, *J. Chem. Inf. Model.* **2015**, *55*, 2562.

[48] RDKit: Open-source cheminformatics, https://www.rdkit.org, (accessed last 31.03.2023). https://doi.org/10.5281/zenodo.6961488

[49] T. A. Halgren, *J. Comput. Chem.* **1996**, *17*, 490.

[50] P. Pracht, F. Bohle, S. Grimme, *Phys. Chem. Chem. Phys.* **2020**, *22*, 7169.

[51] S. Spicher, S. Grimme, *Angew Chem. Int. Ed. Engl.* **2020**, *59*, 15665.

[52] E. W. Bell, Y. Zhang, *J. Cheminform* **2019**, *11*, 40.

[53] B. Hourahine, B. Aradi, V. Blum, F. Bonafé, A. Buccheri, C. Camacho, C. Cevallos, M. Y. Deshaye, T. Dumitrica, A. Dominguez, S. Ehlert, M. Elstner, T. Van Der Heide, J. Hermann, S. Irle, J. Jakowski, J. J. Kranz, C. Köhler, T. Kowalczyk, T. Kubar, I. S. Lee, V. Lutsker, R. J. Maurer, S. K. Min, I. Mitchell, C. Negre, T. A. Niehaus, A. M. N. Niklasson, A. J. Page, et al., *J. Chem. Phys.* **2022**, *157*, 039901.

[54] M. Gaus, A. Goez, M. Elstner, *J. Chem. Theory Comput.* **2013**, *9*, 338.

[55] M. Gaus, X. Lu, M. Elstner, Q. Cui, *J. Chem. Theory Comput.* **2014**, *10*, 1518.

[56] S. Grimme, J. Antony, S. Ehrlich, H. Krieg, *J. Chem. Phys.* **2010**, *132*, 154104.

[57] S. Grimme, S. Ehrlich, L. Goerigk, *J. Comput. Chem.* **2011**, *32*, 1456.

[58] B. Hourahine, B. Aradi, V. Blum, F. Bonafé, A. Buccheri, C. Camacho, C. Cevallos, M. Y. Deshaye, T. Dumitrica, A. Dominguez, S. Ehlert, M. Elstner, T. Van Der Heide, J. Hermann, S. Irle, J. J. Kranz, C. Köhler, T. Kowalczyk, T. Kubar, I. S. Lee, V. Lutsker, R. J. Maurer, S. K. Min, I. Mitchell, C. Negre, T. A. Niehaus, A. M. N. Niklasson, A. J. Page, A. Pecchia, G. Penazzi, et al., *J. Chem. Phys.* **2020**, *152*, 124101.

[59] I. Y. Kanal, J. A. Keith, G. R. Hutchison, *Int. J. Quantum Chem.* **2017**, 118.

[60] S. G. Balasubramani, G. P. Chen, S. Coriani, M. Diedenhofen, M. S. Frank, Y. J. Franzke, F. Furche, R. Grotjahn, M. E. Harding, C. Hättig, A. Hellweg, B. Helmich-Paris, C. Holzer, U. Huniar, M. Kaupp, A.

2309226 (11 of 12)

Marefat Khah, S. Karbalaei Khani, T. Müller, F. Mack, B. D. Nguyen, S. M. Parker, E. Perlt, D. Rappoport, K. Reiter, S. Roy, M. Rückert, G. Schmitz, M. Sierka, E. Tapavicza, D. P. Tew, et al., *J. Chem. Phys.* **2020**, *152*, 184107.

[61] A. Schäfer, H. Horn, R. Ahlrichs, *J. Chem. Phys.* **1992**, *97*, 2571.

[62] S. Grimme, *J. Comput. Chem.* **2006**, *27*, 1787.

[63] C. Lee, W. Yang, R. G. Parr, *Phys. Rev. B Condens Matter.* **1988**, *37*, 785.

[64] P. J. Stephens, F. J. Devlin, C. F. Chabalowski, M. J. Frisch, *J. Phys. Chem.* **2002**, *98*, 11623.

[65] S. H. Vosko, L. Wilk, M. Nusair, *Can. J. Phys.* **1980**, *58*, 1200.

[66] A. Schäfer, C. Huber, R. Ahlrichs, *J. Chem. Phys.* **1994**, *100*, 5829.

[67] O. Treutler, R. Ahlrichs, *J. Chem. Phys.* **1995**, *102*, 346.

[68] K. Eichkorn, O. Treutler, H. Öhm, M. Häser, R. Ahlrichs, *Chem. Phys. Lett.* **1995**, *242*, 652.

[69] K. Eichkorn, F. Weigend, O. Treutler, R. Ahlrichs, *Theor. Chem. Acc.* **1997**, *97*, 119.

[70] F. Weigend, *Phys. Chem. Chem. Phys.* **2006**, *8*, 1057.

[71] M. Sierka, A. Hogekamp, R. Ahlrichs, *J. Chem. Phys.* **2003**, *118*, 9136.

[72] F. Weigend, *Phys. Chem. Chem. Phys.* **2002**, *4*, 4285.

[73] M. Von Arnim, R. Ahlrichs, *J. Comput. Chem.* **1998**, *19*, 1746.

[74] A. Klamt, G. Schüürmann, *J. Chem. Soc., Perkin Trans.* **1993**, *2*, 799.

[75] A. Schäfer, A. Klamt, D. Sattel, J. C. W. Lohrenz, F. Eckert, *Phys. Chem. Chem. Phys.* **2000**, *2*, 2187.

[76] E. F. May, R. C. Miller, A. R. H. Goodwin, *J. Chem. Eng. Data* **2001**, *47*, 102.

[77] R. Bauernschmitt, R. Ahlrichs, *Chem. Phys. Lett.* **1996**, *256*, 454.

[78] R. Bauernschmitt, M. Häser, O. Treutler, R. Ahlrichs, *Chem. Phys. Lett.* **1997**, *264*, 573.

[79] S. Grimme, F. Furche, R. Ahlrichs, *Chem. Phys. Lett.* **2002**, *361*, 321.

[80] F. Furche, D. Rappoport, in *Computational Photochemistry*, 16, (Ed.: M. Olivucci), Elsevier, Amsterdam **2005**.

[81] M. U. M. Uda, *Jpn. J. Appl. Phys.* **1985**, *24*, 284.

[82] M. Uda, Y. Nakagawa, T. Yamamoto, M. Kawasaki, A. Nakamura, T. Saito, K. Hirose, *J. Electron Spectrosc. Relat. Phenom.* **1998**, *88–91*, 767.

[83] H. Yoshida, K. Yamada, J. y. Tsutsumi, N. Sato, *Phys. Rev. B* **2015**, *92*, 075145.

[84] A. Amirav, U. Even, J. Jortner, *J. Chem. Phys.* **1981**, *75*, 2489.

[85] R. R. Gagne, C. A. Koval, G. C. Lisensky, *Inorg. Chem.* **1980**, *19*, 2854.

[86] J. A. Röhr, D. Moia, S. A. Haque, T. Kirchartz, J. Nelson, *J. Phys. Condens. Matter.* **2018**, *30*, 105901.

[87] G. Juska, N. Nekrasas, K. Genevicius, *J. Non-Cryst. Solids* **2012**, *358*, 748.

[88] O. J. Sandberg, M. Nyman, S. Dahlström, S. Sandén, B. Törngren, J.-H. Smått, R. Österbacka, *Appl. Phys. Lett.* **2017**, *110*, 153504.

[89] U. Wurfel, A. Cuevas, P. Wurfel, *IEEE J. Photovoltaics* **2015**, *5*, 461.